Asia-Pacific Journal of Atmospheric Sciences (2019) 55:91–99
https://doi.org/10.1007/s13143-018-00103-8

Online ISSN 1976-7951
Print ISSN 1976-7633

ORIGINAL ARTICLE

Combined Effects of El Niño and the Pacific Decadal Oscillation on Summertime Circulation over East Asia

Sang-Heon Lee[1] · Kyong-Hwan Seo[1] · Minho Kwon[2]

Received: 2 June 2018 / Revised: 6 December 2018 / Accepted: 27 December 2018 / Published online: 5 February 2019
© Korean Meteorological Society and Springer Nature B.V. 2019

Abstract

The El Niño-Southern Oscillation (ENSO) and Pacific decadal oscillation (PDO) are the two major modes of sea surface temperature (SST) variability over equatorial and North Pacific regions, respectively. In this study, the combined effects of the ENSO and PDO on summertime circulation and precipitation fields over East Asia are investigated. Results show that SST forcing associated with a positive ENSO phase intensifies the anticyclonic circulation anomaly over the western North Pacific (WNP) region through a meridionally propagating Rossby wave train or via downward motion due to an overturning circulation stemming from equatorial central Pacific warming. A strong negative SST anomaly over the North Pacific during positive PDO phases increases local meridional temperature gradient and thus induces anomalous westerly winds along 35°N. This wind anomaly forms the northern margin of the anticyclonic circulation anomaly over the WNP. The combined effect of positive ENSO and positive PDO phases strengthens the anticyclonic circulation anomaly more than when these forcings are considered separately. Therefore, to the north of the anomaly, precipitation is enhanced due to the increased moisture flux transport and convergence along the rim of the WNP subtropical high.

Keywords El Niño · The Pacific decadal oscillation · Western North Pacific subtropical high · East Asia precipitation · Combined effect

1 Introduction

The El Niño-Southern Oscillation (ENSO) is a prominent air−sea coupled mode in the tropical Pacific that impacts the global weather and climate system (e.g., Webster et al. 1998). In particular, ENSO is known to influence variations in the Asian monsoon (Rasmusson and Carpenter 1982; Webster and Yang 1992; Ju and Slingo 1995; Wang et al. 2000). As one of the components of the Asian monsoon, the East Asian summer monsoon (EASM) is influenced by ENSO through the variability of the western North Pacific subtropical high (WNPSH) or the Philippine Sea anticyclone (Chang et al. 2000; Lu and Dong 2001; Wang and Zhang 2002; Lee and Seo 2013; Park et al. 2015; Seo et al. 2015). For example, after a peak positive ENSO phase, the WNPSH develops during the summer via air−sea coupling (Wang et al. 2000) and results in a positive rainfall anomaly over East Asia. Other WNPSH formation mechanisms include enhanced sea surface temperature (SST) anomalies in the vicinity of the Maritime continent during La Niña events, which tend to induce anomalous local Hadley circulations over the subtropics (Sui et al. 2007; Park et al. 2010) and SST cooling over the central Pacific, which can lead to the descending Rossby wave or WNPSH slightly to the northwest of the SST forcing region (Wang et al. 2013; Xiang et al. 2013).

In addition to tropical influences, the EASM can be affected by variations in North Pacific SSTs; where the dominant physical mode is the Pacific decadal oscillation (PDO; Mantua et al. 1997). Dong (2016) investigated the impact of the PDO on East Asian precipitation during the non-ENSO period, where anomalous summer precipitation in East China exhibits a tripolar pattern, with increased (decreased) precipitation in the Yangtze-River Valley (North and South China) during the positive PDO phase. Yu et al. (2015) found that positive winter

Responsible Editor: Soon-Il An.

✉ Kyong-Hwan Seo
khseo@pusan.ac.kr

[1] Department of Atmospheric Sciences, Division of Earth Environmental System, Pusan National University, Busan, South Korea

[2] Korea Institute of Ocean Science & Technology, Busan, South Korea

SST anomalies (SSTA) in the eastern subtropical Pacific propagated to the tropics in the following summer, leading to warming in the eastern tropical Pacific Ocean. This in turn induces an enhanced WNPSH and, thus, increased precipitation over southern China. Seo et al. (2015) showed that the SST cooling over the North Pacific (i.e., positive PDO phase) can induce a cold anomaly over northeast Asia and the North Pacific, which leads to increases in the meridional gradient of equivalent potential temperature and baroclinicity. This in turn can cause favorable conditions for intense precipitation over northern East Asia. Notwithstanding, further research is necessary to investigate these mechanisms more clearly and to investigate the direct effects of midlatitude SSTA.

Although ENSO and PDO exhibit different time scales, interannual variations of temperature and rainfall can be affected by the both modes (Chan and Zhou 2005; Feng et al. 2014; Kim et al. 2014; Wu and Mao 2016). Previous research by Feng et al. (2014) indicated that, when El Niño is in phase with the PDO, low-level circulation anomalies are characterized by an anticyclone over the Philippine Sea and a cyclone over Japan, inducing an anomalous tripolar rainfall pattern in China. PDO modulation of the ENSO effect on spring precipitation in southern China was examined by Wu and Mao (2016). They showed that, during El Niño under a positive PDO phase, southern China experienced above-average precipitation induced by an enhanced subtropical anticyclone over the western North Pacific (WNP) and an intensified subtropical westerly jet over the southern Tibetan Plateau. Yoon and Yeh (2010) demonstrated that northeast Asian precipitation was intensified when El Niño and PDO were in phase. They argued that PDO could modulate the relationship between El Niño and northeast Asian precipitation though the Eurasian teleconnection pattern.

Accordingly, it is necessary to investigate how PDO modulates El Niño's impact on the circulation and precipitation over northeast Asia. In this study, the combined effect of ENSO and PDO during the summer is examined. Results show that their combined influence strengthens the circulation and precipitation signal, thus enhancing the predictability of the EASM. In section 2, data and methods are introduced, section 3 describes the results, and section 4 summarizes our findings.

2 Data and Methods

To identify the relevant SST variation on intraseasonal time scale, observed daily SST data are used in this study. These are derived from the National Oceanic and Atmospheric Administration Optimum Interpolation Sea Surface Temperature version 2 data set (OISSTv2; Reynolds et al. 2002). Daily zonal and meridional winds and geopotential heights from ERA-Interim (Dee et al. 2011) reanalysis data were used. Pentad-mean Global Precipitation Climatology Project (GPCP; Huffman et al. 1997; Adler et al. 2012) data is used for precipitation. Due to the lack of continuous data coverage, the common data period 1982–2014 is used.

In this paper, the averaged Niño4 [5°S − 5°N, 160°E −150°W] index during June and July is used to represent ENSO. Use of Niño4 instead of Niño3.4 is based on the results of previous studies which demonstrated that precipitation over northeastern Asia during July is enhanced by central Pacific SST warming (Yeh et al. 2009; Seo et al. 2015). Note also that since Niño4 includes a more western portion of the equatorial SST index regions compared to Niño3 or Niño3.4 and the equatorial western Pacific is climatologically the warm region, even weak anomalous warm SST can induce a deep convection and thus atmospheric response.

The summertime PDO is defined as the first spatial pattern of empirical orthogonal function (EOF) analysis for the North Pacific domain (20° − 60°N, 120°E−120°W) during the extended summer May–October. The PDO index is defined by the first principal component (PC) time series as in Mantua et al. (1997). We compare this PC time series with the PDO index by Mantua et al. (1997) (available online at http://jisao.washington.edu/pdo/PDO.latest). The correlation coefficient is 0.97, which is statistically significant at 95% confidence level. PDO is predominantly characterized by Pacific decadal-to-interdecadal SST variability; however, it shows significant variability on interannual time scales as well (Schneider and Cornuelle 2005; Fig. 1). Both the Niño4 and PDO indices are normalized, and 0.43 standard deviations (~33.3%) are selected as the criterion for distinguishing a strong positive phase (Fig. 1). Even if the interannual time series of the PDO and Niño4 correlate each other at the level of ~0.4, which is statistically significant at 95% confidence level, their contributing roles differ because the PDO mainly represents extratropical variation, while ENSO does tropical variation, as shown in this study. Strong ENSO and PDO years are shown in Table 1. To remove high frequency variation, an 8-pentad running mean is applied for all data.

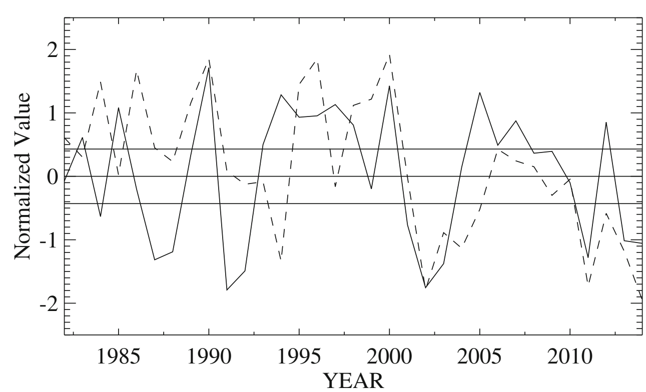

Fig. 1 Time series of the Niño4 SST index (solid line) and PDO index (dashed line) from mid-June to July for the period 1982–2014. Two horizontal lines denote the 0.43 and − 0.43 standard deviations

Table 1 Classification of years based on ENSO and PDO phases for the period 1982–2014

	+PDO (10)	−PDO (11)	Neutral (12)
+ENSO (14)	1987, 1992, 1993, 1995, 1997, 2014	1991, 2002, 2009	1982, 1990, 1994, 2003, 2004
−ENSO (10)	1984	1999, 2000, 2008, 2010, 2011	1985, 1988, 1989, 1998
Neutral (9)	1983, 1986, 1996	2001, 2012, 2013	2005,2006,2007

The number of selected cases is shown in the parenthesis

A linear baroclinic model (LBM; Watanabe and Kimoto 2000) is used with a horizontal resolution of T42 and 20 vertical levels in sigma coordinates. Based on linearized primitive equations, the LBM produces a near steady-state atmospheric dynamical response to prescribed diabatic heating after day 20.

3 Results

Figure 2a shows the composite of anomalous rainfall during mid-June to July for El Niño events only. The equatorial region shows a typical El Niño-related pattern with a positive precipitation anomaly in the equatorial western Pacific and a negative precipitation anomaly over the Maritime continent. A weak (but statistically significant) negative precipitation anomaly appears in the WNP (140°E, 20°N); however, there is no significant signal in East Asia. During the positive PDO phase (Fig. 2b), enhanced (decreased) precipitation is apparent in the equatorial central Pacific (the Maritime continent). This pattern is similar to that of El Niño; however its intensity is weaker (Fig. 2b). The WNP region (150°E, 20°N) also shows a weak (but statistically significant) negative precipitation anomaly, while East Asia, including the Korean peninsula, does not display any distinct signal.

When El Niño is in phase with PDO (Fig. 2c), precipitation anomalies are strengthened over the tropical Pacific, the Maritime continent and the WNP. More importantly, over East Asia, a slanted band of precipitation anomaly is shown with a meridionally opposite pattern over Korea and central-north China, and the Yangtze River valley extending to the south of Japan.

To identify the formation mechanism of this precipitation pattern, we examine the 850-hPa geopotential height and wind fields. Under El Niño conditions (Fig. 2d), the warm SSTA in the central equatorial Pacific drives enhanced deep atmospheric convection and westerly wind anomalies. Enhanced rainfall anomalies in the equatorial central Pacific induce a cyclonic Rossby anomaly (140°E, 10°N; Gill 1980) and an anticyclonic anomaly to the northeast of the Philippine Sea through a meridionally propagating Rossby wave. When PDO is in a positive phase (Fig. 2e), a westerly wind anomaly occurs in the equatorial Pacific that is relatively weak as compared to the El Niño case (Fig. 2d) and an anticyclonic circulation anomaly appears slightly northeast of the Philippine Sea and this is driven by a mechanism similar to the El Niño case.

When the positive PDO and El Niño appear together (Fig. 2f), the stronger westerly wind anomaly occurs over the equatorial western Pacific, and more importantly, both the cyclonic anomaly near 10°N and the anticyclonic anomaly are stronger than those cases where positive PDO and El Niño appear independently. To the northwest of this anticyclonic circulation anomaly, increased precipitation occurs in the Yangtze River and south of Japan due to moisture transport induced by southerly and southwesterly flows. Furthermore, decreased precipitation occurs over the Korean peninsula, which is attributed to northerly dry advection caused by a weak cyclonic circulation anomaly centered over Japan [140°E, 35°N].

To establish the impact of the equatorial and midlatitude dominant modes of the Pacific, the spatial patterns of atmospheric and oceanic variables are examined using regression analysis. An SST field regressed against Niño4 shows positive SST anomalies over the equatorial central and eastern Pacific (Fig. 3a), as would be expected. In response to this warming, the positive precipitation anomaly (Fig. 3b) appears to the west of this forcing and the negative precipitation anomaly develops over the Maritime continent as a part of Walker circulation.

In the subtropics and midlatitudes, the negative precipitation anomaly develops over the WNP region (Fig. 3b). This anomaly appears to be initiated by the strong convection associated with anomalous precipitation over the equatorial central western Pacific. The central Pacific warming intensifies the low-level cyclonic circulation anomaly over the WNP in Fig. 3c through a Gill-type response (Gill 1980). To the north of this cyclonic anomaly (i.e., northeast of the Philippine Sea), an anticyclonic circulation anomaly is formed by a meridionally propagating Rossby wave train forced by the central Pacific warming. Therefore, the central Pacific El Niño causes subsidence over the WNP, which intensifies the WNPSH (Fig. 3c). This may be a compensating overturning circulation response caused by strong convection over the equatorial central

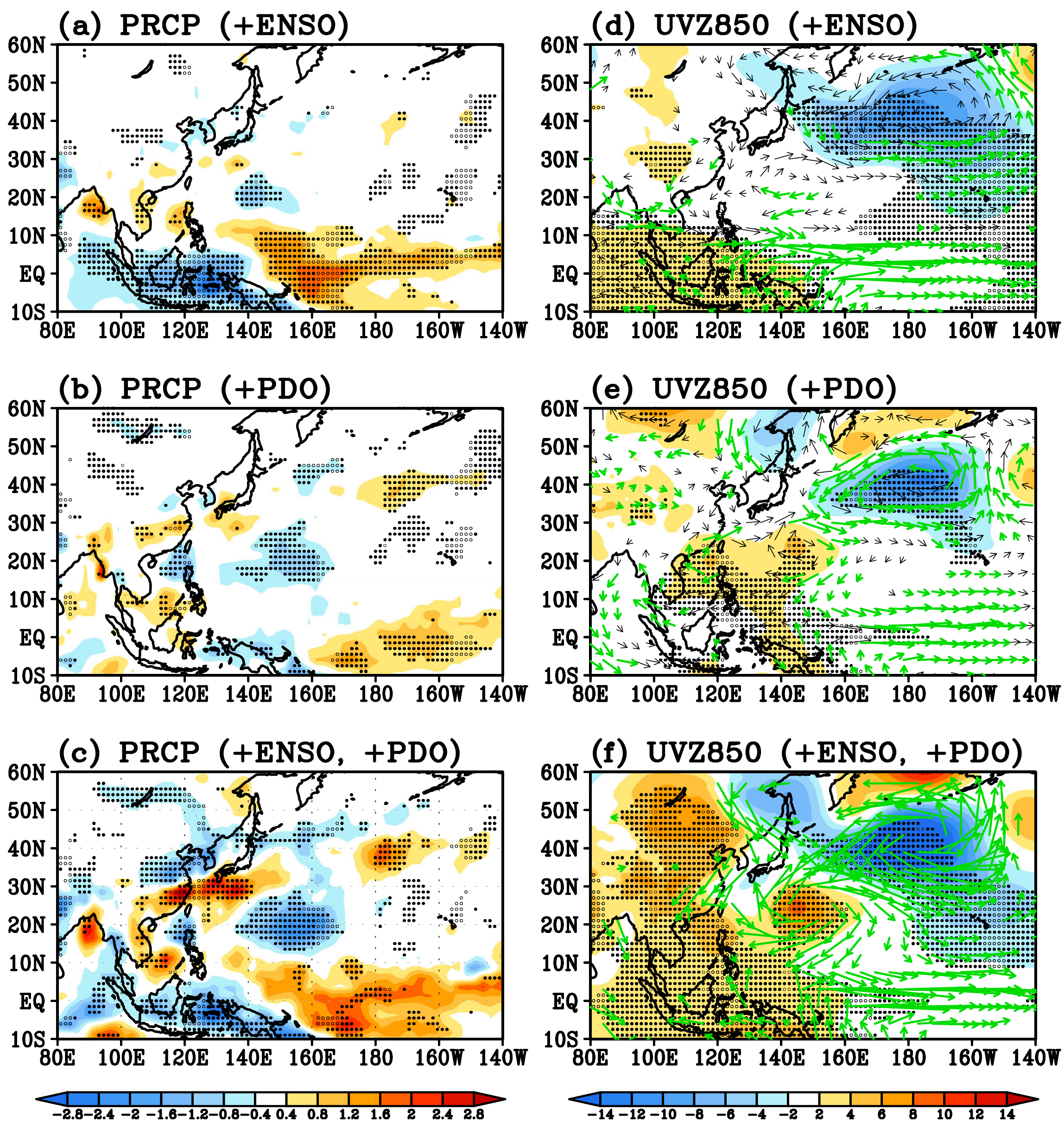

Fig. 2 Composite maps of precipitation (mm day^{-1}, color) from mid-June to July for **a** positive ENSO, **b** positive PDO, and **c** both positive ENSO and PDO. Panels (**d**) to (**f**) are the same as (**a**) to (**c**), but for geopotential height (m, color) and horizontal wind (m s^{-1}) at 850 hPa. Dotted areas in (**a** − **c**) represent those regions exceeding the 90% confidence level. Thick vectors in (**d** − **f**) are significant at the 90% confidence level

Pacific (140° − 170°E) as shown in the meridional vertical cross section (Fig. 3d).

Figure 4a shows SSTAs regressed against the summertime PDO index. A typical PDO-related SST pattern is apparent over the North Pacific; cold anomalies along 40°N extending from 150°W to the eastern coast of Asia, and warm anomalies over the northeastern Pacific extending northwestward along the North American coast and southwestward to the central tropical Pacific (Mantua et al. 1997). A weak warming signal in the equatorial central Pacific, while not statistically significant, induces an easterly wind anomaly along 15°N over the Philippine Sea as a Rossby wave response. A more peculiar feature is the development of a westerly wind anomaly along 35°N (Fig. 4c), which is caused by a strong negative SSTA over the North Pacific (Fig. 4a). The cooling strengthens the meridional gradient of the SSTA because the climatological midlatitude SST field has a strong north-south gradient over the North Pacific (Fig. 4d). This enhanced SST gradient causes the atmospheric meridional temperature gradient and the latter induces westerly flow in the subtropics and midlatitudes (Sampe et al. 2010; Lee and Seo 2013; Park et al. 2015). Through the thermal wind balance, the westerly flow becomes more enhanced with height (not shown). A lead-lag correlation is calculated for the meridional SST gradient and the zonal wind anomaly at 850 hPa. The result (Fig. 5) shows a peak correlation of 0.38 at pentad lag −2 (where the

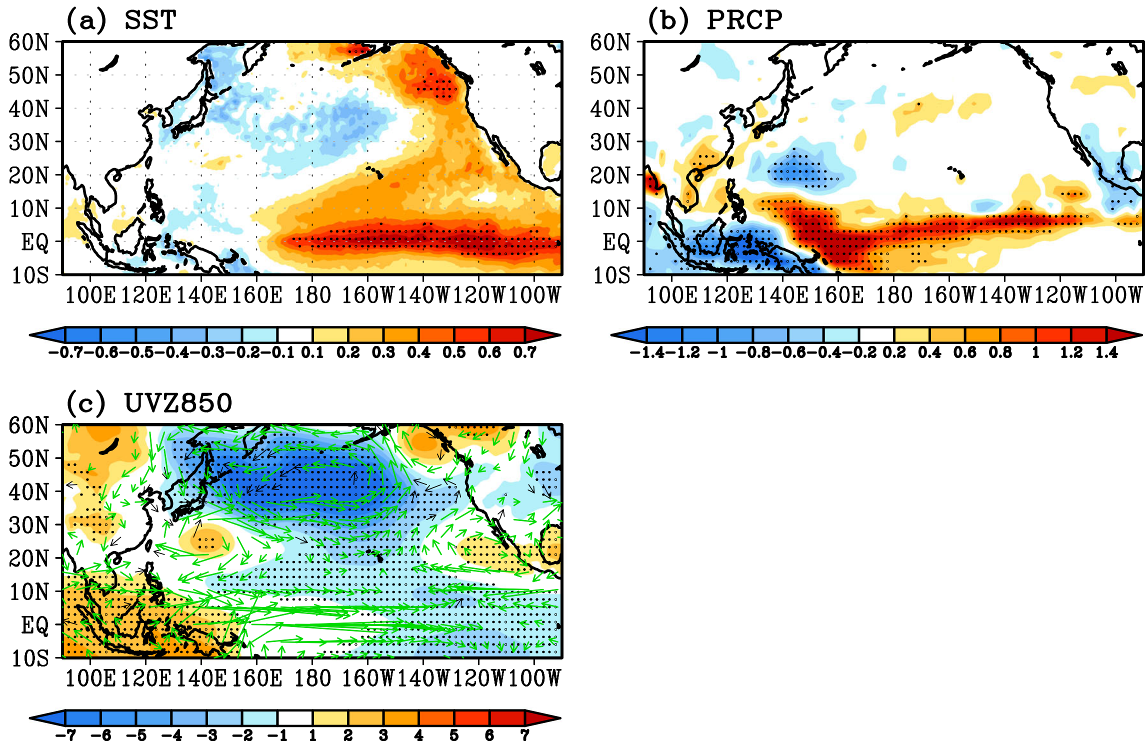

Fig. 3 Regressed anomaly fields of **a** SST, **b** precipitation, **c** geopotential height and horizontal wind at 850 hPa, and **d** streamlines of the flow in a latitude–height cross section averaged from 110° − 140°E, with respect to the Niño4 index (mid-June to July). Dotted areas in (**a** − **c**) represent those regions exceeding the 90% confidence level and thick vectors in (**c**) are significant at a 90% confidence level. Shading in (**d**) indicates areas where one of the wind components is statistically significant at the 90% confidence level

correlation is statistically significant at 90% confidence level obtained by Monte Carlo experiment with 1000 random trials), implying that the strengthening of the meridional SST gradient leads to the enhancement of the westerly flow. All

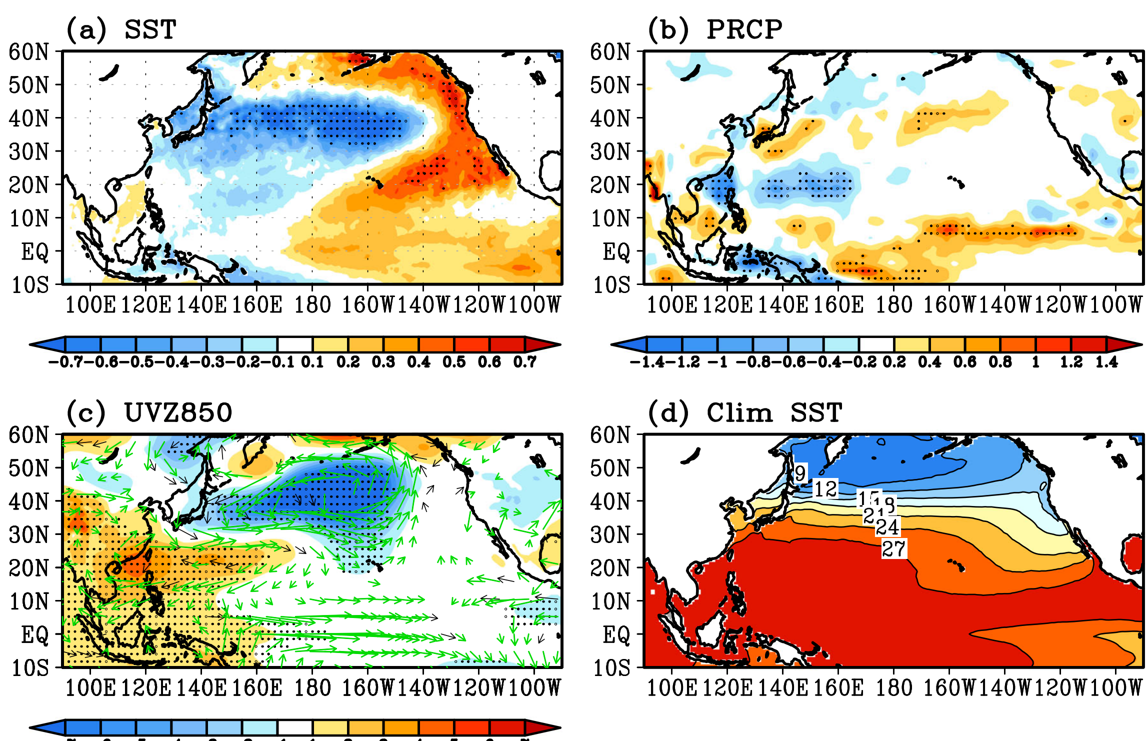

Fig. 4 **a** − **c** Same as in Fig. 3, except for the PDO index. **d** Climatological SST (°C) from mid-June to July

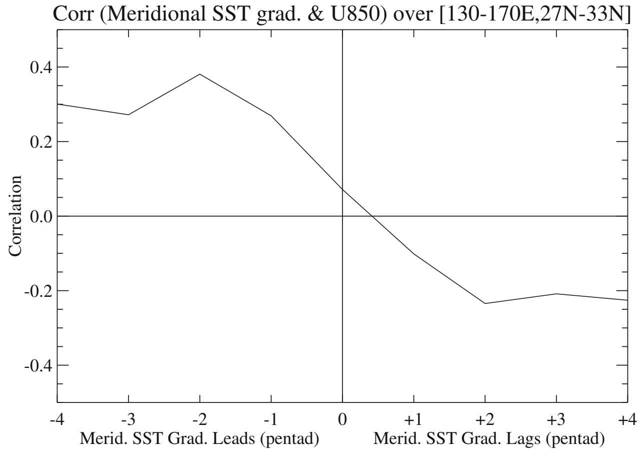

Fig. 5 Lead-lag correlation between meridional SST gradient and zonal wind anomaly at 850 hPa averaged over [130° − 170°E, 27° − 33°N]

these analyses suggest that eddy momentum flux convergence does not play a role since an isolated low-level zonal wind enhancement does not appear.

Related to both the westerly wind anomaly along 35°N and the easterly wind anomaly along 15°N at 850 hPa, a significant anticyclonic circulation anomaly develops over the WNP, implying a strengthening of the WNPSH or its westward extension. This WNPSH induces the decreased precipitation anomaly to the north of the Philippine Sea. The westerly wind anomaly along the 35°N can also be generated by this negative precipitation anomaly forcing (not shown). Hence, the negative precipitation anomaly over the Philippine Sea and the westerly wind anomaly to the north of it can sustain through the positive feedback between diabatic forcing and wind anomalies. The weak warming over the equatorial central Pacific (Fig. 4a) only slightly contributes to the enhancement of the anticyclonic anomaly.

The role of the westerly zonal wind anomaly and negative SSTA over the North Pacific, which can induce an anticyclonic circulation anomaly over the WNP, requires verification. To establish whether the westerly wind anomaly along 35°N can produce the anticyclonic circulation anomaly over the subtropical region, precipitation, geopotential height, and horizontal wind at 850 hPa are regressed against the zonal wind anomaly index averaged over [130° − 170°E, 27° − 33°N] (Figs. 6a and c) during mid-June to July. The anticyclonic (cyclonic) circulation anomaly is apparent to the south (north) of the westerly anomaly at approximately 30°N (Fig. 6c). Consistent with the circulation anomaly, the decreased precipitation (Fig. 6a) appears over the Philippine Sea with the increased precipitation immediately south of Japan.

To determine if this westerly wind anomaly can be attributed to the midlatitude cold SSTA, we regress the same variables against the SSTA index averaged over the cooling region (Fig. 4a) in the North Pacific [150° − 210°E, 35° − 45°N] (Figs. 6b and d). Development of the westerly wind anomaly is apparent along 30°N (Fig. 6d) in addition to the anomalous, but relatively weaker, anticyclone in the Philippine Sea (Fig. 6d). The precipitation anomaly (Fig. 6b), consistent with the wind field, is negative over this region; however, it is also weaker. This may imply that the midlatitude SSTA does not directly produce the high-pressure anomaly over the Philippine Sea; however, the westerly wind anomaly caused by the response of the midlatitude cold SSTA does produce the anticyclonic circulation anomaly over the Philippine Sea. Comparing the sensitivity of these responses using model experiment warrants further studies.

It is apparent that both ENSO and PDO produce the anomalous anticyclone over the Philippine Sea, and their combined effect strengthens the anomaly. Furthermore, they strengthen together the positive precipitation anomaly to the north of the anticyclonic anomaly (i.e., to the south of Japan) and the negative precipitation anomaly to the north of the anticyclonic anomaly (i.e., over the Korean peninsula; Fig. 2c). The enhanced anticyclonic circulation signal over the Philippine Sea during the simultaneous positive phases of ENSO and PDO (Fig. 2f) results from the combined effect of enhancement in the subtropical easterly wind anomaly along 15°N due to ENSO and enhancement in the extratropical westerly wind anomaly along 35°N due to PDO.

The meridionally opposite precipitation anomalies seen over the Korean peninsula and to the south of Japan are consistent with the findings of Ham et al. (2016), where positive precipitation anomalies related to SSTA over the northern central Pacific induced an atmospheric teleconnection extending in a northwest-southeast direction. In their study, the atmospheric teleconnection is shown to generate geopotential height anomalies over these two regions similar to ours. In our case, the cyclonic circulation anomaly is formed over Japan (Fig. 2f), and as such, northerly dry wind advection leads to the negative precipitation anomaly over the Korean peninsula (Fig. 2c).

Our analysis indicates that the two different forcing anomalies contribute to the development and strengthening of the anticyclonic circulation anomaly over the WNP area, which ultimately leads to the enhanced and suppressed precipitation to the north and south of the circulation anomaly, respectively. To verify the atmospheric response to diabatic heating associated with the positive phases of both ENSO and PDO, simple linear model experiments are performed using LBM. The tropical heating anomaly is used to represent ENSO-related forcing, while the subtropical cooling anomaly is used to represent PDO-related forcing. The diabatic heating profile is calculated using an apparent heat source (Q1) following Yanai et al. (1973). Horizontally, heating has a cosine squared profile in an elliptical region, and a vertical gamma profile is used with a maximum heat source of 400 hPa ($\sigma = 0.45$). The maximum imposed heating (cooling) is 2.5 (−1.5) K day^{-1} for ENSO (PDO). This imposed profile approximately mimics observations.

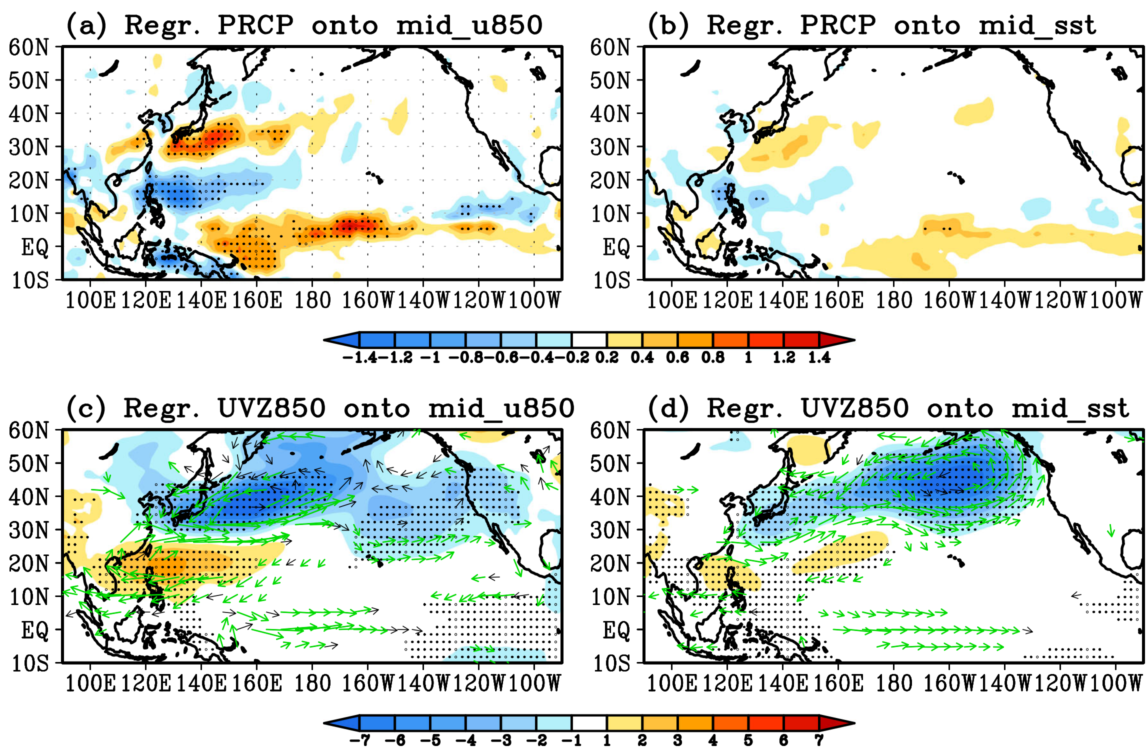

Fig. 6 **a** Precipitation anomaly and **c** geopotential height and horizontal wind anomaly at 850 hPa regressed against the index time series of zonal wind anomaly at 850 hPa averaged over 130° − 170°E, 27–33°N. **b** and **d** are the same as **a** and **c** but against the SSTA index averaged over the North Pacific [150° − 210°E, 35° − 45°N]. Dotted areas represent those regions exceeding the 90% confidence level and the thick vectors in (**c** − **d**) are significant at a 90% confidence level

Figure 7a shows the day 20–25 averaged 850-hPa geopotential height response to the ENSO-related tropical forcing centered at [150°E, 5°N]. Similar to observations, a cyclonic circulation anomaly is produced over the Philippine Sea and an anticyclonic circulation anomaly is formed to the north of the cyclonic anomaly. The cyclonic anomaly is a Gill-type Rossby wave response (Gill 1980) as anticipated, and the anticyclonic anomaly is generated by a meridionally propagating Rossby wave train (Fig. 7a).

For the PDO forcing, diabatic cooling is placed over the subtropical region centered at [160°E, 20°N] (Fig. 7b). The anomalous anticyclone is produced as a Rossby wave response to the suppressed convective heating, which corresponds to the strengthening WNPSH. The combined effect of tropical heating and subtropical cooling (Fig. 7c) induces much stronger anticyclonic circulation responses in the subtropical region, indicating that both forcing anomalies result in the strengthening of the WNPSH and therefore impact the East Asian precipitation field. Because LBM is a linear model, the summation of the circulation responses from each experiment (not shown) produces approximately the same response to that shown in Fig. 7c.

4 Summary and Discussion

In this paper, we examine how ENSO and PDO, the two major modes of equatorial and north Pacific SST variability, respectively, affect the circulation and precipitation fields over East Asia and the western North Pacific. SST forcing associated with the positive phase of ENSO (Figs. 3b and c) produces an intensified anticyclonic circulation anomaly over the WNP region through a meridionally propagating Rossby wave train or via downward motion due to an overturning circulation forced by equatorial central Pacific warming.

On the other hand, the strong negative SSTA over the North Pacific during the positive PDO (Fig. 4a) increases the meridional temperature gradient due to this enhanced SST gradient, leading to anomalous westerly winds along 35°N (Fig. 4c). This wind anomaly forms the northern part of the anticyclonic circulation anomaly over the WNP. The combined effect of ENSO and PDO results in a more peculiar WNPSH circulation anomaly (Fig. 2f) as compared to the separate forcing cases. The key driver affecting East Asia is the anticyclonic circulation anomaly over the WNP and the northern part of the anomaly is strengthened by PDO-related westerly wind anomalies and the southern part is enhanced by ENSO-related easterly wind anomalies formed as a Rossby

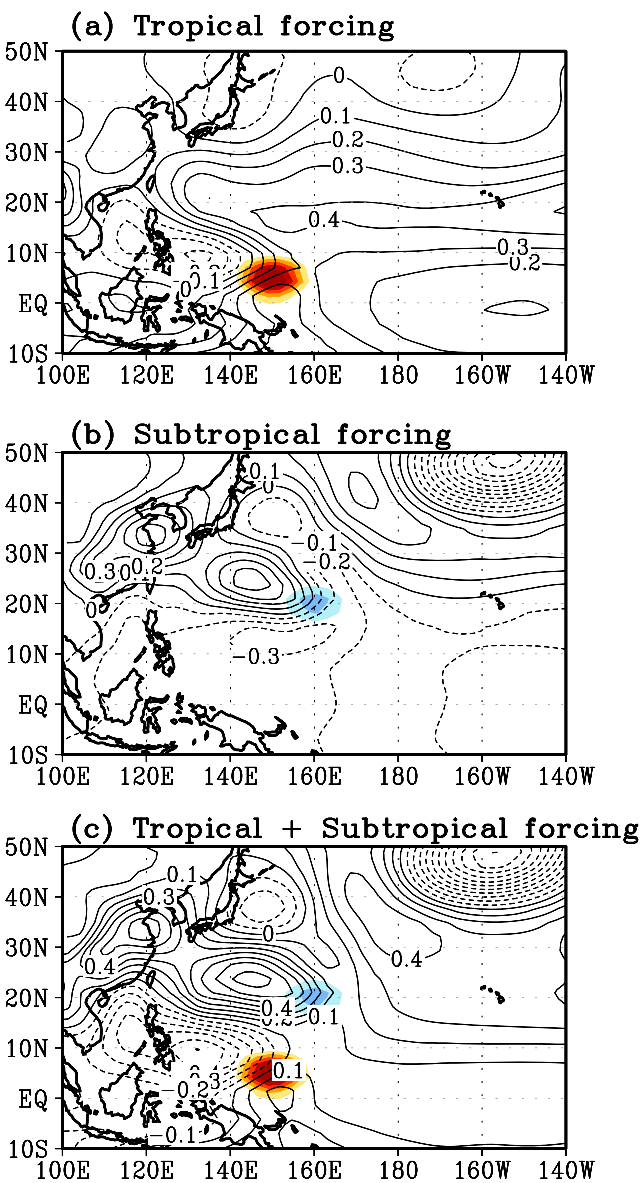

Fig. 7 Model experiments for **a** tropical, **b** subtropical, and **c** both tropical and subtropical forcing. Contours show 850-hPa geopotential heights. The shading represents the region of the imposed heating (red) and cooling (blue) anomalies

wave cyclonic circulation response. Therefore, to the north of the WNPSH, the precipitation is enhanced due to increased moisture flux transport and convergence along the northwestern and northern margins of the WNPSH. We speculate that anomalous diabatic forcing south of Japan could generate the negative precipitation anomaly over the Korean peninsula by inducing a cyclonic circulation anomaly to the north of the forcing, and therefore dry northerly advection into central-north China and the northern Korean peninsula.

To slightly increase the number of the events selected, ERA40 data are combined with ERAI data so now data period spans from 1958 to 2014 (57 yrs). (The former data are for period from 1958 through 2002 and the latter data for 2003 onwards). In this case, monthly data for June and July are used for composite (cf. the present study used daily data and the composite is for mid-June to July average). Even if only one more year is included to original +PDO/+ENSO, three more cases are included for +PDO and five more cases for +ENSO. The circulation responses for +PDO and + PDO/+ENSO (not shown) are very similar to those shown in Fig. 2e and f, respectively. The other combinations such as +PDO/–ENSO and + PDO/neutral ENSO demonstrate rather different circulation fields compared to +PDO/+ENSO combination (not shown).

A series of general circulation model experiments will be conducted to gain more insights into the formation of the precipitation field associated with the phases of ENSO and PDO in the future. Furthermore, since the positive PDO is dominant during the data period used in this study, the characteristics and dynamics related to the negative PDO have not been explored. Using an extended-period data or a series of long-free simulations of coupled model, more detailed characteristics of combined effect of PDO and ENSO need to be examined. For the latter case, climate model with a high fidelity in simulating both the ENSO and PDO may be required to establish more confident results.

Acknowledgements This work was supported by the National Research Foundation of Korea (NRF) grant funded by the Korea government (MSIP) (No. NRF-2018R1A2A2A05018426) and the KMA Research and Development Program under Grant KMI 2018–01012. We would like to thank the two anonymous reviewers for their helpful comments and suggestions.

Publisher's Note Springer Nature remains neutral with regard to jurisdictional claims in published maps and institutional affiliations.

References

Adler, R.F., Gu, G., Huffman, G.J.: Estimating climatological bias errors for the global precipitation climatology project (GPCP). J. Appl. Meteorol. Climatol. **51**, 84–99 (2012). https://doi.org/10.1175/JAMC-D-11-052.1

Chan, J.C.L., Zhou, W.: PDO, ENSO and the early summer monsoon rainfall over South China. Geophys. Res. Lett. **32**, L08810 (2005). https://doi.org/10.1029/2004GL022015

Chang, C.-P., Zhang, Y., Li, T.: Interannual and interdecadal variations of the east Asian summer monsoon and tropical Pacific SSTs. Part I: roles of the subtropical ridge. J. Clim. **13**, 4310–4325 (2000)

Dee, D., et al.: The ERA-interim reanalysis: configuration and performance of the data assimilation system. Q. J. R. Meteorol. Soc. **137**, 553–597 (2011). https://doi.org/10.1002/qj.828

Dong, X.: Influences of the Pacific decadal oscillation on the East Asian summer monsoon in non-ENSO years. Atmos. Sci. Lett. **17**, 115–120 (2016)

Feng, J., Wang, L., Chen, W.: How does the East Asian summer monsoon behave in the decaying phase of El Niño during different PDO phases? J. Clim. **27**, 2682–2698 (2014). https://doi.org/10.1175/JCLI-D-13-00015.1

Gill, A.E.: Some simple solutions for heat induced tropical circulation. Q. J. R. Meteorol. Soc. **106**, 447–462 (1980)

Ham, Y.-G., Kug, J.-S., Yeh, S.-Y., Kwon, M.: Impacts of two distinct teleconnection patterns induced by Western Central Pacific SST anomalies on Korean temperature variability during the early boreal summer. J. Clim. **29**, 743–759 (2016). https://doi.org/10.1175/JCLI-D-15-0406.1

Huffman, G.J., et al.: The Global Precipitation Climatology Project (GPCP) combined precipitation dataset. Bull. Amer. Meteor. Soc. **78**, 5–20 (1997). https://doi.org/10.1175/1520-0477(1997)078,0005:TGPCPG.2.0.CO;2

Ju, J., Slingo, J.M.: The Asian summer monsoon and ENSO. Q. J. R. Meteorol. Soc. **121**, 113–1168 (1995)

Kim, J.-W., Yeh, S.-W., Chang, E.-C.: Combined effect of El Niño-southern oscillation and Pacific decadal oscillation on the East Asian winter monsoon. Clim Dyn. **42**, 957–971 (2014). https://doi.org/10.1007/s00382-013-1730-z

Lee, S.-E., Seo, K.-H.: The development of a statistical forecast model for Changma. Weather. Forecast. **28**, 1304–1321 (2013). https://doi.org/10.1175/WAF-D-13-00003.1

Lu, R., Dong, B.W.: Westward extension of North Pacific subtropical high in summer. J. Meteor. Soc. Japan. **79**, 1229–1241 (2001)

Mantua, N.J., Hare, S.R., Zhang, Y., Wallace, J.M., Francis, R.C.: A Pacific interdecadal climate oscillation with impacts on salmon production. Bull. Am. Meteorol. Soc. **78**, 1069–1079 (1997)

Park, J.-Y., Jhun, J.-G., Yim, S.-Y., Kim, W.-M.: Decadal changes in two types of the western North Pacific subtropical high in boreal summer associated with Asian summer monsoon/ El Niño–southern oscillation connections. J. Geophys. Res. **115**, D21129 (2010). https://doi.org/10.1029/2009JD013642

Park, H.-L., Seo, K.-H., Son, J.-H.: Development of a dynamics-based statistical prediction model for the Changma onset. J. Clim. **28**, 6647–6666 (2015). https://doi.org/10.1175/JCLI-D-14-00502.1

Rasmusson, E.M., Carpenter, T.H.: Variations in tropical sea surface temperature and surface wind fields associated with the southern oscillation/El Niño. Mon. Weather. Rev. **110**, 354–384 (1982)

Reynolds, R.W., Rayner, N.A., Smith, T.M., Stokes, D.C., Wang, W.: An improved in situ and satellite SST analysis for climate. J. Clim. **15**, 1609–1625 (2002)

Sampe, T., Nakamura, H., Goto, A., Ohfuchi, W.: Significance of a midlatitude SST frontal zone in the formation of a storm track and an eddy-driven westerly jet. J. Clim. **23**, 1793–1814 (2010)

Schneider, N., Cornuelle, B.D.: The forcing of the Pacific decadal oscillation. J. Clim. **18**, 4355–4373 (2005)

Seo, K.-H., Son, J.-H., Lee, J.-Y., Park, H.-S.: Northern east Asian monsoon precipitation revealed by airmass variability and its prediction. J. Clim. **28**, 6221–6233 (2015)

Sui, C.-H., Chung, P.-H., Li, T.: Interannual and interdecadal variability of the summertime western North Pacific subtropical high. Geophys. Res. Lett. **34**, L11701 (2007). https://doi.org/10.1029/2006GL029204

Wang, B., Zhang, Q.: Pacific–east Asian teleconnection. Part II: how the Philippine Sea anomalous anticyclone is established during El Niño development. J. Clim. **15**, 3252–3265 (2002)

Wang, B., Wu, R.G., Fu, X.H.: Pacific-East Asian teleconnection: how does ENSO affect east Asian climate? J. Clim. **13**, 1517–1536 (2000)

Wang, B., Xiang, B., Lee, J.-Y.: Subtropical high predictability establishes a promising way for monsoon and tropical storm predictions. PNAS. **110**, 2718–2722 (2013). https://doi.org/10.1073/pnas.1214626110

Watanabe, M., Kimoto, M.: Atmosphere-ocean thermal coupling in the North Atlantic: a positive feedback. Q. J. R. Meteorol. Soc. **126**, 3343–3369 (2000). https://doi.org/10.1002/qj.49712657017

Webster, P.J., Yang, S.: Monsoon and ENSO: selectively interactive systems. Q. J. R. Meteorol. Soc. **118**, 877–926 (1992)

Webster, P.J., Magana, V.O., Palmer, T.N., Shukla, J., Tomas, R.A., Yanai, M., Yasunari, T.: Monsoons: processes, predictability, and the prospects for prediction. J. Geophys. Res. **103**(C7), 14,451–14, 510 (1998)

Wu, X., Mao, J.: Interdecadal modulation of ENSO-related spring rainfall over South China by the Pacific decadal oscillation. Clim. Dyn. **47**, 3203–3220 (2016)

Xiang, B., Wang, B., Yu, W., Xu, S.: How can anomalous western North Pacific subtropical high intensify in late summer? Geophys. Res. Lett. **40**, 2349–2354 (2013). https://doi.org/10.1002/grl.50431

Yanai, M., Esbensen, S., Chu, J.-H.: Determination of bulk properties of tropical cloud clusters from large-scale heat and moisture budgets. J. Atmos. Sci. **30**, 611–627 (1973)

Yeh, S.-W., Kug, J.-S., Dewitte, B., Kwon, M.-H., Kirtman, B., Jin, F.-F.: El Niño in a changing climate. Nature. **461**, 511–514 (2009). https://doi.org/10.1038/nature08316

Yoon, J., Yeh, S.-W.: Influence of the Pacific decadal oscillation on the relationship between El Niño and the northeast Asian summer monsoon. J. Clim. **23**, 4525–4537 (2010). https://doi.org/10.1175/2010JCLI3352.1

Yu, L., Furevik, T., Otterå, O.H., Gao, Y.: Modulation of the Pacific decadal oscillation on the summer precipitation over East China: a comparison of observations to 600-yrs control run of Bergen climate model. Clim Dyn. **44**, 475–494 (2015). https://doi.org/10.1007/s00382-014-2141-5